16th World Conference on Earthquake Engineering, 16WCEE 2017

Santiago Chile, January 9th to 13th 2017

Paper N° 1631 (Abstract ID)

Registration Code: S-E1463254871

PSHAe (PROBABILISTIC SEISMIC HAZARD ASSESSMENT ENHANCED): THE CASE OF ISTANBUL

M. Stupazzini(1), M. Infantino(2), A. Allmann(3), M.Kaeser(4), R. Paolucci(5), I. Mazzieri(6), C. Smerzini(7)

(1) Munich RE, Germany, MStupazzini@munichre.com
(2) MSc student, Politecnico di Milano, maria.infantino@mail.polimi.it
(3) Munich RE, Germany, AAllmann@munichre.com
(4) Munich RE, Germany, MKaeser@munichre.com
(5) Department of Civil and Environmental Engineering, Politecnico di Milano, Italy, roberto.paolucci@polimi.it
(6) Laboratoty for Modeling and Scientific Computing, Department of Mathematics, Politecnico di Milano, ilario.mazzieri@polimi.it
(7) Department of Civil and Environmental Engineering, Politecnico di Milano, Italy, chiara.smerzini@polimi.it

Abstract

The Probabilistic Seismic Hazard Analysis (PSHA) only relying on ground motion prediction equations (GMPEs) tends to be insufficiently constrained at short distances and data only partially account for the rupture process, seismic wave propagation and three-dimensional (3D) complex configurations. Given a large and representative set of ground shaking scenarios from 3D physics-based numerical simulations, analyzing the resulting database from a statistical point of view and implementing the results as a generalized attenuation function (GAF) into the classical PSHA might be an appealing way to deal with this problem [1]. Nonetheless, the limited amount of computational resources or time available tend to pose substantial constraints to a broad application of the previous method. Furthermore, the method is only partially suitable for taking into account the spatial correlation of ground motion as modelled by each forward physics-based simulation (PBS).

In this context, we envision a streamlined and novel approach for enhanced PSHA ("PSHAe") in large urban areas, alternative to the previous method, based on the integration into the probabilistic framework of a limited number of deterministic scenarios, being the latter wisely chosen and associated to a probability of occurrence.

The experience gathered in the past year regarding 3D modelling of seismic wave propagation in complex alluvial basin (see e.g.: [2], [3] and [4]) allowed us to enhance the choice of simulated scenarios in order to explore the variability of ground motion, preserving the full spatial correlation necessary for risk modelling.

3D numerical modelling of scenarios occurring along the North Anatolian Fault in the proximity of Istanbul are carried out through the spectral element code SPEED (http://speed.mox.polimi.it). The results are introduced in a PSHA based code, exploiting the capabilities of this methodology.

Keywords: physics-based earthquake scenario; high-performance computing in elastodynamics; reinsurance policy in seismic risk mitigation

1. Introduction

Forward physics-based modelling has achieved in the recent time an impressive level of reliability (see e.g. [5], [3], [4]) allowing, in certain range of frequencies, the use of synthetic ground motions or scenarios (e.g.: peak ground map obtained from the numerical simulation of an earthquake) as alternative or complementary tool to more traditional techniques mainly based on observed data (e.g., NGA database: http://peer.berkeley.edu/ngawest2/).

In spite of the advantages of using this methodology, some severe drawbacks, like the (i) covered range of frequencies, (ii) geological and geotechnical data required and (iii) computational costs, have been always pointed out as a reasonable justification to limit the use of this kind of methodology only to few selected case study. In order to prove that the limitations previously listed are losing their status of "cogent argument" and to promote a wider use of forward physics-based modelling, the following activities have been undertaken:

(i) creating (and maintaining) a "state-of-the-art" code for the study of elastodynamic wave propagation problems. The open-source code SPEED (SPectral Elements in Elastodynamics with Discontinuous Galerkin; http://speed.mox.polimi.it) described in [6] and [7], succeeded in quantifying the spatial variability of the ground motion induced by key parameters like (a) complex deep soft soil structure, (b) directivity effect and (c) soil non-linearities;

(ii) creating (and maintaining) a freely available repository of physics-based simulations (PBS); the large set of footprint scenarios has been identified worldwide in order to cover locations with a severe impact for the society, mainly focusing on areas that have not been already investigated;

(iii) allowing researchers to freely use SPEED (and all its products) and to contribute to its further development and use.

The use of PBS in a probabilistic seismic hazard analysis (PSHA) environment is clearly one of the most promising areas of advancement in the frame of natural hazard assessment ([8]). Villani et al.(ref. [1]) presented an appealing way to deal with this problem: starting from a large and representative set of 3D scenarios, analysing the resulting database from a statistical point of view and finally implementing the results as a generalized attenuation model into the classical PSHA. Nonetheless, the limited amount of computational resources or time available tend to pose substantial constraints in a broad application of the previous method and furthermore the method is only partially suitable for properly taking into account the spatial correlation of ground motion as modelled by each forward physics-based simulation.

Given that, this work presents a streamlined and alternative implementation of the previous approach, aiming at (i) selecting wisely a limited number of representative scenarios and (ii) associating each of them with a probability of occurrence. The experience gathered over the past years regarding 3D ground shaking scenarios allowed us to enhance the choice of those latter in order to explore the variability of ground motion, preserving the full spatial correlation necessary for risk modelling.

Because of the serious threat posed to the city of Istanbul by the North Anatolian Fault (NAF), this region has been chosen as the case study in order to present the above mentioned methodology.

Initially a short description of the area investigated and some details about the novel approach implemented to construct broadband accelerograms are provided; a detailed version is illustrated in a companion paper submitted to the 16WCEE conference (Paolucci et al., "3D Physics-based earthquake scenarios in Istanbul for seismic risk assessment"). Thereafter, the dataset of physics-based scenarios is compared against classical GMPE and some conclusions are drawn regarding the expected level of shaking for large events occurring along the NAF in the proximity of Istanbul. Furthermore, a detailed analysis of the residual is proposed in order to assess the reliability of our synthetic dataset and finally the results of our PSHA are presented in term of shaking maps for certain return period, aiming at highlighting the differences between a classical analysis based on GMPE or a PSHAe based on PBSs.

2. Application to the Istanbul case study

The computational model of Istanbul region extends over an area of 165x100 km^2 down to 30 km depth (see Fig. 1) and consists of 2,257,482 hexahedral elements, resulting in approximately 475 million degrees of freedom, using a fourth order polynomial approximation degree and a size variable conforming mesh (from a minimum of 180 m, on the top surface, up to 600 m at 2 km depth and reaching 1800 m in the underlying layers). A set of 51 physics-based scenarios (PBSs), generated by seismic rupture of the North Anatolian Fault (NAF), are carried out using a computational approach which involves the following three main tools: (i) the computer code SPEED ([6]); (ii) a pre-processing tool, i.e. a rupture generator, to produce a set of kinematic slip models along a given fault within a prescribed magnitude according to two kinematic source models, i.e. Herrero and Bernard (1994) (ref. [1]), referred to as "HB94", and Crempien and Archuleta (2015) (ref. [10]), "CA15"; (iii) a post-processing tool to generate broadband (BB) ground motions starting from the results of SPEED, applicable only to the low frequency range. For each simulation a time step equal to 0.001 s has been chosen for the time marching scheme and a total observation time T = 60 s has been considered. Simulated scenarios were generated by varying the magnitude, from 7.0 up to 7.4, the source rupture model (HB94 or CA15), the kinematic slip distribution, the hypocenter location and the location of the rupture area. In Table 1 synthetic scenarios are listed grouped for magnitude and source model.

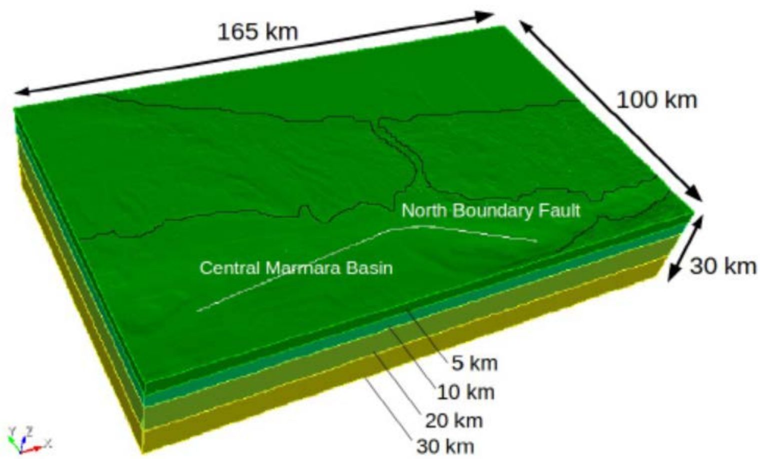

Fig. 1 - Computational domain of the Istanbul region.

Table 1 – Simulated scenarios grouped for magnitude and source

Source/Mw	7.0	7.2	7.4
HB94	20	10	6
CA15	4	7	4

A more detailed description of the model, the computational approach and the deterministic ground-shaking scenarios simulated, are illustrated in a companion paper submitted to the 16WCEE conference (Paolucci et al.,"3D Physics-based earthquake scenarios in Istanbul for seismic risk assessment").

3. Statistical analysis of numerical results

We aim in this section at illustrating some relevant features of the simulated scenarios, focusing on the effect of magnitude. For this purpose attenuation relationships purely calibrated on the synthetic data set of simulated ground motions for Istanbul area have been elaborated and compared with ground motion prediction equations available in literature. For the sake of clarity in the following, the former will be called synthetic ground motion prediction equation (SGMPE) while the latter will be referred to using the classical acronym GMPE.

In order to explain the differences observed at higher magnitude (Mw ≥ 7.2) between GMPEs and SGMPEs, the onset of possible forward directivity conditions has been investigated.

3.1 Synthetic vs classical GMPEs

The SGMPE functional form adopted is particularly simple (see Eq.(1)), nevertheless it is suitable to account for the key parameters affecting ground motion estimates, such as magnitude, distance from the fault and soil class. Furthermore the SGMPE can be obviously calibrated using a single synthetic event or a certain set of them (respectively represented with green and blue line in the following plots). It should be considered that each simulation produces many thousands of three components seismograms at a uniform grid of observation points at ground surface. Therefore, fitting this large dataset with a simple functional form allows one to "summarize" the information coming from the synthetics into a more concise and readable form.

$$\mathbf{log_{10}(GM) = a - b \cdot log_{10}(R + h)} \qquad (1)$$

In the Eq. (1) *GM* is the ground-motion intensity (such as peak ground motion or response spectra at selected periods), *R* is the rupture distance defined as the minimum distance to the fault, *a* and *h* are parameters estimated in Matlab using the function *lsqcurvefit*, while *b* is chosen constant and equal to 1, implicitly assuming a decay of the ground motion proportional to R^{-1}. The parameters *a* and *h* are estimated independently for any class of soil, implying a dependence of the SGMPEs on magnitude, distance and soil class, similarly to classical GMPEs.

Fig. 2 shows, on the left panel, the comparison between the PGVgmh (gmh = geometric mean of horizontal components) values, for a single synthetic scenario (namely the 507) of Mw 7.0 and soil class with $V_{S,30}$ of 500 m/s (magenta dots) and the SGMPE calibrated on this single event (green lines). On the right panel the comparison between the PGVgmh resulting from the entire synthetic dataset of scenarios with Mw 7.0 and HB94 source model (in total 20 scenarios) and soil class with $V_{S,30}$ of 500 m/s (magenta dots) and the associated SGMPE (blue lines) is presented.

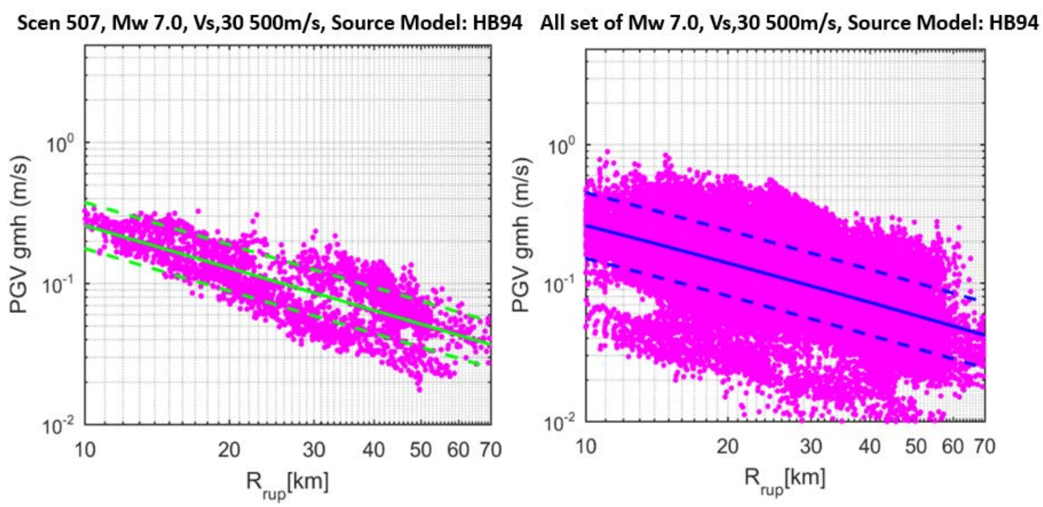

Fig. 2 – *left panel*: synthetic PGVgmh observed for one scenario with Mw 7.0 (magenta dots) and the corresponding SGMPE mean (+/-) 1 standard deviation (solid and dashed green lines respectively). *Right panel*: synthetic PGVgmh observed for the entire set of synthetic scenarios with Mw 7.0 (magenta dots) and the corresponding SGMPE mean (+/-) 1 standard deviation (solid and dashed blue lines respectively). The selected class of soil has a $V_{S,30}$ = 500 m/s and the scenarios are generated with an HB94 source.

As already mentioned, different SGMPEs have been compared against classical GMPEs. Fig. 3 presents the PGVgmh obtained by means of SGMPEs calibrated on the synthetic data set of magnitude 7.0, 7.2 and 7.4 and HB94 source type (blue line), against the analogous Chiou and Youngs 2008 (red line), hereinafter CHYO08 (ref[11]).

In the bottom panel the same comparison is illustrated for Mw 7.2 and generated with an CA15 source. Note that this comparison refers to results obtained on soil class with $V_{S,30}$ of 500 m/s. In the figure the dispersion bands ±σ of both CHYO08 and the SGMPE, calibrated using all synthetic scenarios with a given magnitude, are also shown (dashed lines); the green line shows the SGMPE calibrated on the synthetics of a single event independently.

It is worth noting that SGMPE calibrated with the Mw 7.0 PBSs agrees very well with the CHYO08 prediction, while on the contrary the SGMPEs, based on Mw 7.2 and 7.4 dataset, presents a clear shift against CHYO08. A similar behavior is found for all soil classes and also against the GMPE proposed by Cauzzi et al 2014 (hereinafter CAEA14, ref [12]).

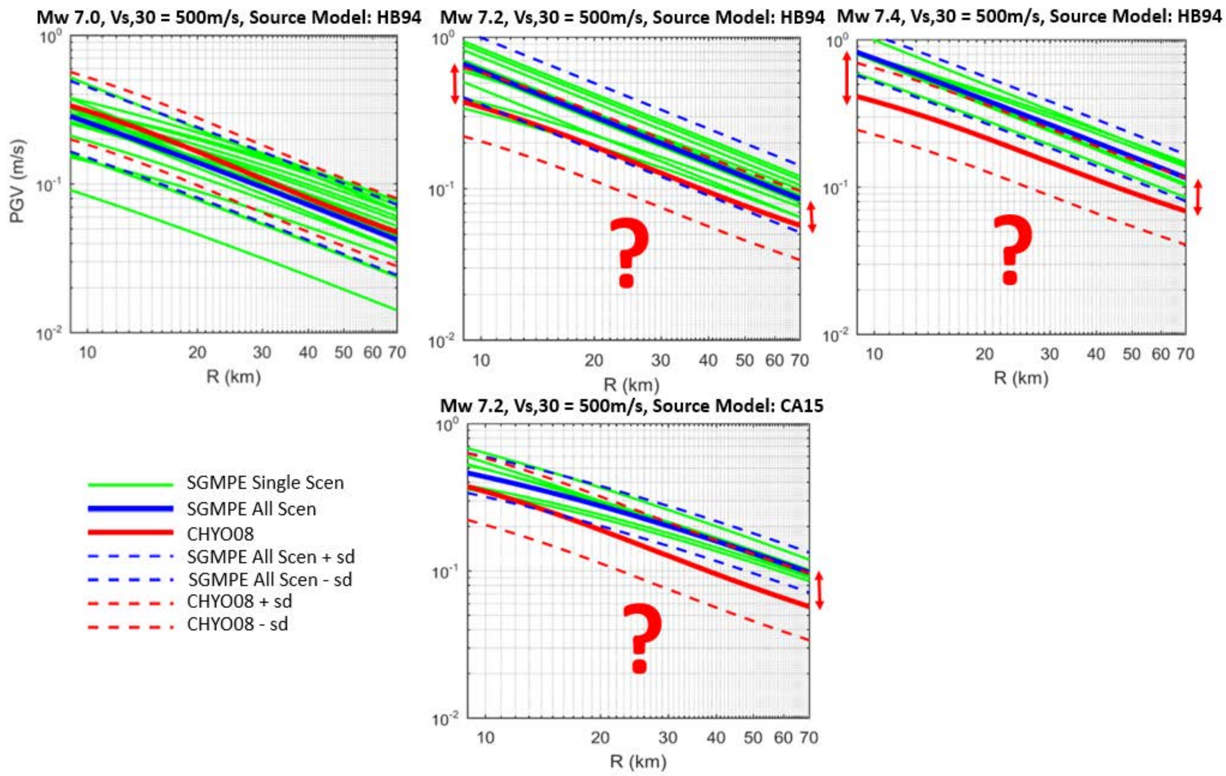

Fig. 3 – comparison between CHYO08 average PGVgmh (red line) +/- σ (dashed red lines) and SGMPEs based on PBSs with magnitude 7.0 (top left), 7.2 (top center) and 7.4 (top right) and HB94 source type. Below analogously CHYO08 against the SGMPEs based on PBSs with magnitude 7.2 (bottom center) and CA15 source type. All the panels shows the soil class with $V_{S,30}$ = 500 m/s.

3.2 Geometrical and physical explanation

The reason of this mismatch between SGMPEs and GMPEs passing from Mw 7.0 to Mw 7.2 can be explained if we consider the particular position of Istanbul and the geometrical configuration of the causative fault system. The examined section of the NAF might be sketched as three segments, with a total length of around 150 km, and Istanbul is located on the convergence of the two outer segments (see Fig. 5).

Due to the limited length of a magnitude 7.0 event (around 40 km), directive, anti-directive or bilateral events, are clearly distinguishable (see Fig. 5 top panels). On the contrary for higher magnitudes, it is no longer possible to distinguish these different directivity conditions essentially because the seismic rupture will have a dimension almost comparable to the entire section of the NAF considered. The combinations of slip distribution and hypocenter position will mostly result to be directive to Istanbul (bottom panels of Fig. 5) or bilateral.

The GMPE of Bray and Rodriguez-Marek (2004) (hereinafter BRRO04,see ref. [13]), based only on near field seismograms presenting clear forward-directivity effect, offers us the chance to prove if our explanation is meaningful or not. In fact, in Fig. 4 it might be noted that the SGMPEs based on PBSs with magnitude 7.2 and 7.4, average (blue line) and +/- σ (blue dashed line) are in very good agreement with BRRO04 mean (black solid line) and the standard deviation (black dashed line).

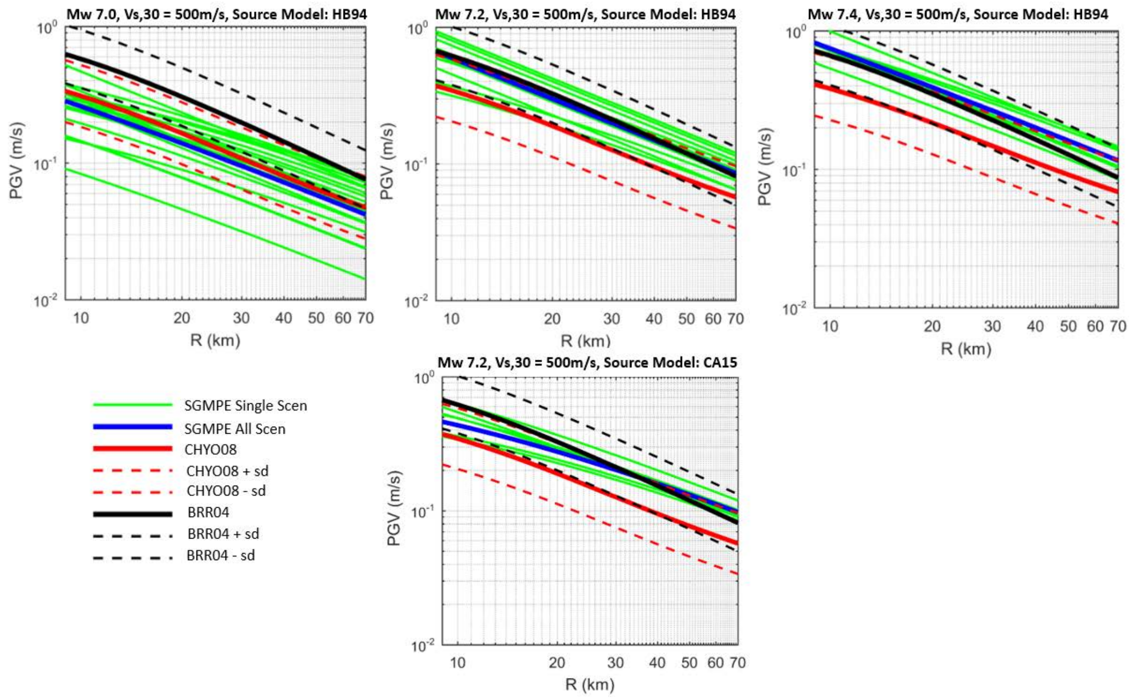

Fig. 4 - comparison between CHYO08 average PGVgmh (red line) +/- σ (dashed red lines), BRRO04 average PGVgmh (black line) +/- σ (dashed black lines) and SGMPEs based on PBSs (blue line) with magnitude 7.0 (top left), 7.2 (top center) and 7.4 (top right) and HB94 source type. Below analogously CHYO08, BRRO04 against the SGMPEs based on PBSs with magnitude 7.2 (bottom center) and CA15 source type. All the panels shows the soil class with $V_{S,30}$ = 500 m/s.

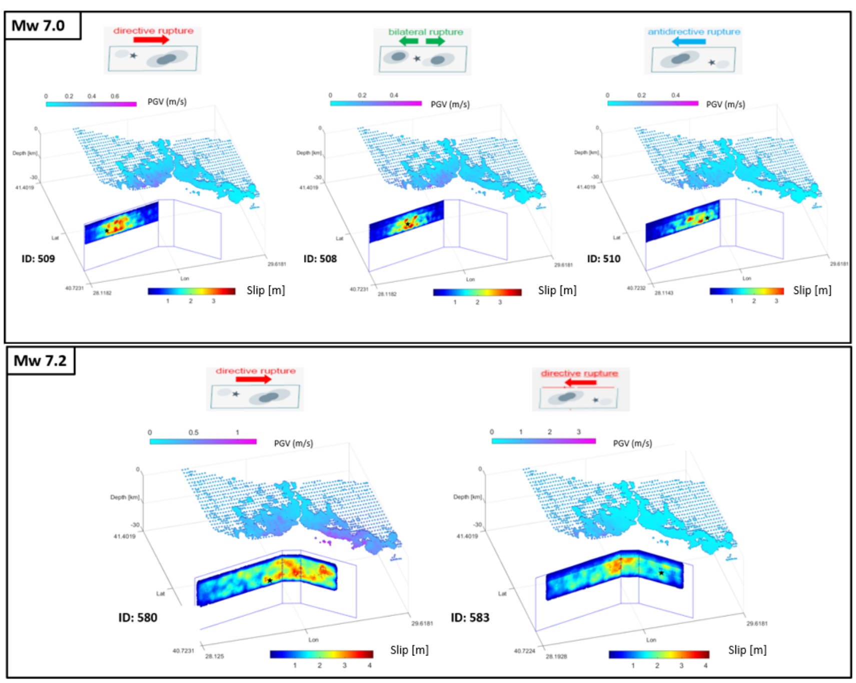

Fig. 5 - Different combinations of hypocenter position and slip distribution for scenarios of Mw 7.0 (top panels) and scenarios of Mw 7.2 (bottom panels). While for scenarios with magnitude 7.0 is possible to distinguish between directive (left top panel, ID 509), bilateral (central top panel, ID: 508) and anti-directive (right top panel, ID: 510), this is no longer possible for scenarios with magnitude 7.2.

4. Analysis of residuals

Goal of this paragraph is to analyze the residuals in order to test the reliability of the simulations by comparing our results with those from other studies. For the sake of clarity it is worth to summarise the key relationships for residual analysis of ground motion values, described by Strasser et al. (2009) and Al Atik et al. (2010) (ref [14] and [15])

4.1 Method of ground motion residual analysis

Denoting as Y_{esk} and M_{esk} respectively the base natural or base 10 logarithm of the observed and predicted value of ground motion for each station (s) from each event (e) at each period (k), the total model residuals is calculated as the misfit between observed (or simulated) values and that predicted by the model:

$$\mathbf{R_{esk} = Y_{esk} - M_{esk} = c_k + \delta B_{ek} + \delta W_{esk}} \quad (2)$$

where, c_k is the mean offset representing the average bias of the actual data relative to the model predictions, δB_{ek} is the between event (also called inter-event) residuals and δW_{esk} is the within-event (also called intra-event) residuals.

$$\mathbf{\delta B_{ek\_TOT} = c_k + \delta B_{ek}} \quad (3)$$

The total inter-event residuals Eq.(3), represents the average shift of the observed ground motion in an individual earthquake, e, from the median predicted by a GMPE. Hence considering NS stations recording the event, δB_{ek_TOT} is calculated as the average misfit between observations (synthetics in our case) and predictions for earthquake e, using a GMPE:

$$\mathbf{\delta B_{ek\_TOT} = \frac{1}{NS}\sum_{s=1}^{NS}(Y_{esk} - M_{esk})} \quad (4)$$

δB_{ek_TOT} is assumed to be normally distributed random variable with c_k mean and variance τ^2, while δB_{ek} is assumed to be normally distributed random variable with 0 mean and variance τ^2. δW_{esk}, is the misfit between an individual observation at station s and the earthquake-specific median prediction of the model (M_{esk}) plus the between-event term (δB_{ek_TOT}). In other words δW_{esk} represents the difference between an individual observation and the event-corrected median estimate.

Since the regression model is calibrated with simulated values, the average bias of the data relative to the model predictions (c_k) is 0 (i.e. $\delta B_{ek\_TOT} = \delta B_{ek}$). Assuming δB_{ek} and δW_{esk} normally distributed random variables with respective variance τ^2 and ϕ_{SS}^2.

The average within-event residual at station s is referred to as the site term because represents the average site correction term and is defined as:

$$\mathbf{\delta S2S_s = \frac{1}{NEs}\sum_{s=1}^{NS}\delta W_{esk}} \quad (5)$$

where NEs is the number of events recorded at the station s; $\delta S2Ss$ has zero mean and variance ϕ^2_{S2S}, under the assumption of no bias in the records obtained at each station.

Finally the term $\phi_{SS,s,}$ referred as the single-station event corrected standard deviation (event- corrected sigma) of the within-event residuals, is defined as:

$$\boldsymbol{\phi_{SS,s} = \sqrt{\frac{\sum_{e=1}^{NE_s}(\delta W_{es} - \delta S2S_s)^2}{NE_s - 1}}} \quad (6)$$

Then if δBe and δWes are mutually independent for station s, the standard deviation of the total residuals at station s is given by:

$$\boldsymbol{\sigma_{SS,s} = \sqrt{\phi_{SS,s}^2 + \tau^2}} \quad (7)$$

Moreover the event–corrected single station standard deviation ϕ_{SS} for the entire dataset can be computed by averaging the $\phi_{SS,s}$ for each station s over all the stations and attributing equal weight to each of them:

$$\boldsymbol{\phi}_{\mathbf{SS}} = \sqrt{\frac{\sum_{s=1}^{NS}\sum_{e=1}^{NE_s}(\delta W_{es} - \delta S2S_s)^2}{\sum_{s=1}^{NS} NE_s - 1}} \tag{8}$$

Finally, assuming that δB_{ek} and δW_{esk} are statistically indipendent variables, then the single-station standard deviation (sigma) is calculated as:

$$\boldsymbol{\sigma}_{\mathbf{SS}} = \sqrt{\boldsymbol{\phi}_{\mathbf{SS}}^2 + \boldsymbol{\tau}^2} \tag{9}$$

4.2 Distribution of total inter-event residuals of PGA with magnitude

Fig. 6 presents the distribution δB_{ek_TOT} of PGA for the model CHYO08 (grey dots) with magnitude, as obtained by Gülerce et al. (2016) (see ref[16]), who proposed an analysis of the residuals, using the Turkish strong ground motion dataset. The dataset considered by the authors is dominated by events with magnitude smaller than 6.5 and only two events (namely the Duzce and Kocaeli earthquakes of 1999) shows a magnitude larger than 7.0; on the contrary our PBSs presents only events with Mw ≥ 7.0, therefore covering a magnitude interval that is poorly represented inside the Turkish strong ground motion dataset. The red stars and lines represent respectively the mean ±σ of δB_{ek_TOT} calculated with the synthetic data of the present study and for the model of CHYO08. Our synthetic results seem to show that the trend highlighted by the authors continues even for higher magnitude.

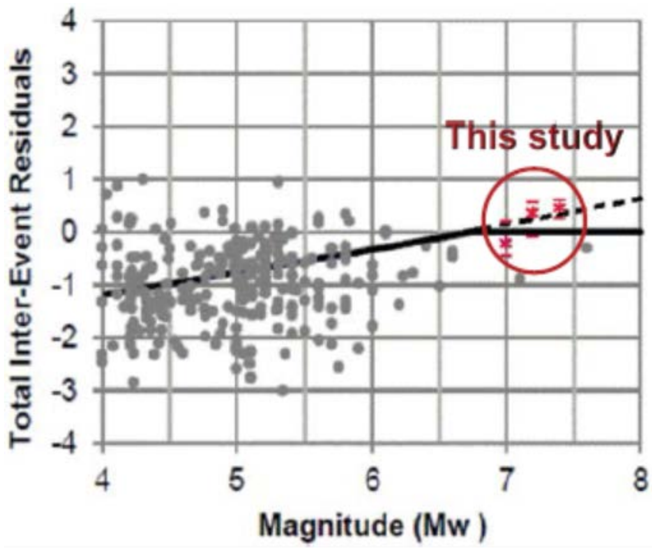

Fig. 6 - Distribution of δB_{ek_TOT} of PGA of the Turkish dataset for the CHYO08 (grey dots) with magnitude ([16]). Red stars and lines represent respectively the mean +/- standard deviation of the δB_{ek_TOT} calculated with the synthetic data of the present study and for the model of CHYO08.

4.3 Single-station standard deviation analysis

The single station standard deviation components of our simulations are shown on the left panel of Fig. 7. Moreover the right panel provides a comparison with the single station standard deviation components calculated by Chen and Faccioli (2013) (see ref [17]) on the basis of a dataset composed by 551 records obtained in 65 earthquakes recorded by 14 strong motion stations in 2010 and 2012 from events with Mw > 4.0 in the Canterbury Plains (New Zealand) and the GMPE of Faccioli et al. 2010 in an improved version (see [18]). It is interesting to note that the results are extremely consistent although they come from two different regions.

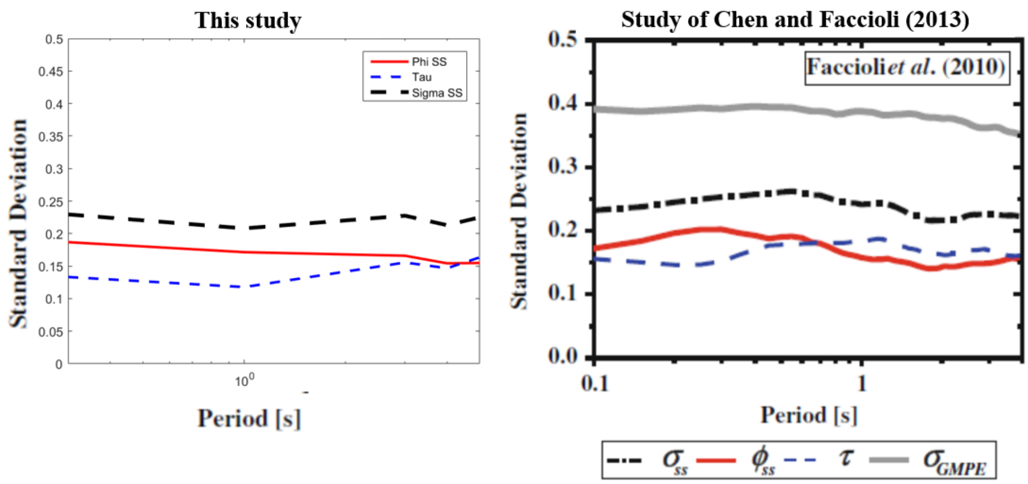

Fig. 7 – (Left panel) components of single – station standard deviation of simulations of this study; (right panel) components of single – station standard deviation of the Canterbury database (ref[6]).

5. Process development and methodological advancement in view of a PSHAe

The PSHA introduced by Cornell (1968) (ref [19]) involves three steps: (i) definition of the seismic-hazard source model(s), (ii) specification of the ground motion predictive equation(s), GMPEs, and (iii) the probabilistic calculation. As already proposed by different authors (see e.g.: [20] and [1]), combining the probabilistic and deterministic approaches in the hazard analysis is feasible and allows to overcome some of the limitations inherent in the deterministic and Cornell classical approaches.

Referring to the PSHA, for a particular site, the seismic-hazard source model provides N earthquakes, each of which has an associated magnitude, location and annual occurrence rate. For a given magnitude and distance, the GMPE provides the distribution of possible ground-motions usually considering also the soil conditions at each site. In the envisioned methodology, we propose to make direct use of PBSs, by choosing wisely certain scenarios out of a set of many that pose a significant threat for a given site. This allows to incorporate important physical effects in the PSHA, such as the radiation pattern, the fault geometry, the directivity effect, the 3D seismic response of soft soil and soil non linearity.

In our PSHA implementation the calculation of the distribution of ground motion is, as normally happens, controlled by a logic-tree. Classical GMPE or PBSs might be easily chosen, simply reassigning logic-tree branch weights (see figure below).

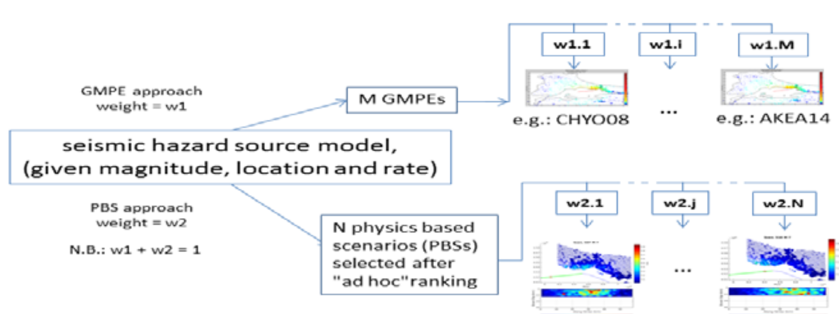

Fig. 8 – Integration of selected PBSs into a classical logic tree based approach.

In the following figure is presented a preliminary comparison between GMPE (left column) and PBSs (right column) based seismic hazard in terms of hazard maps of PGVgmh [m/s] for two different return periods for the area of Istanbul. Only the NAF and earthquakes with magnitude ranging between 7.0 and 7.4 are taken into account. As previously mentioned, the computations are easily performed simply changing the logic-tree branch weights. If a GMPE based hazard map is computed the whole weight will be assigned to the GMPE branch and zero weight to the PBS branch. Vice versa, if PBSs based computation is required. Obviously even mixed computations are allowed.

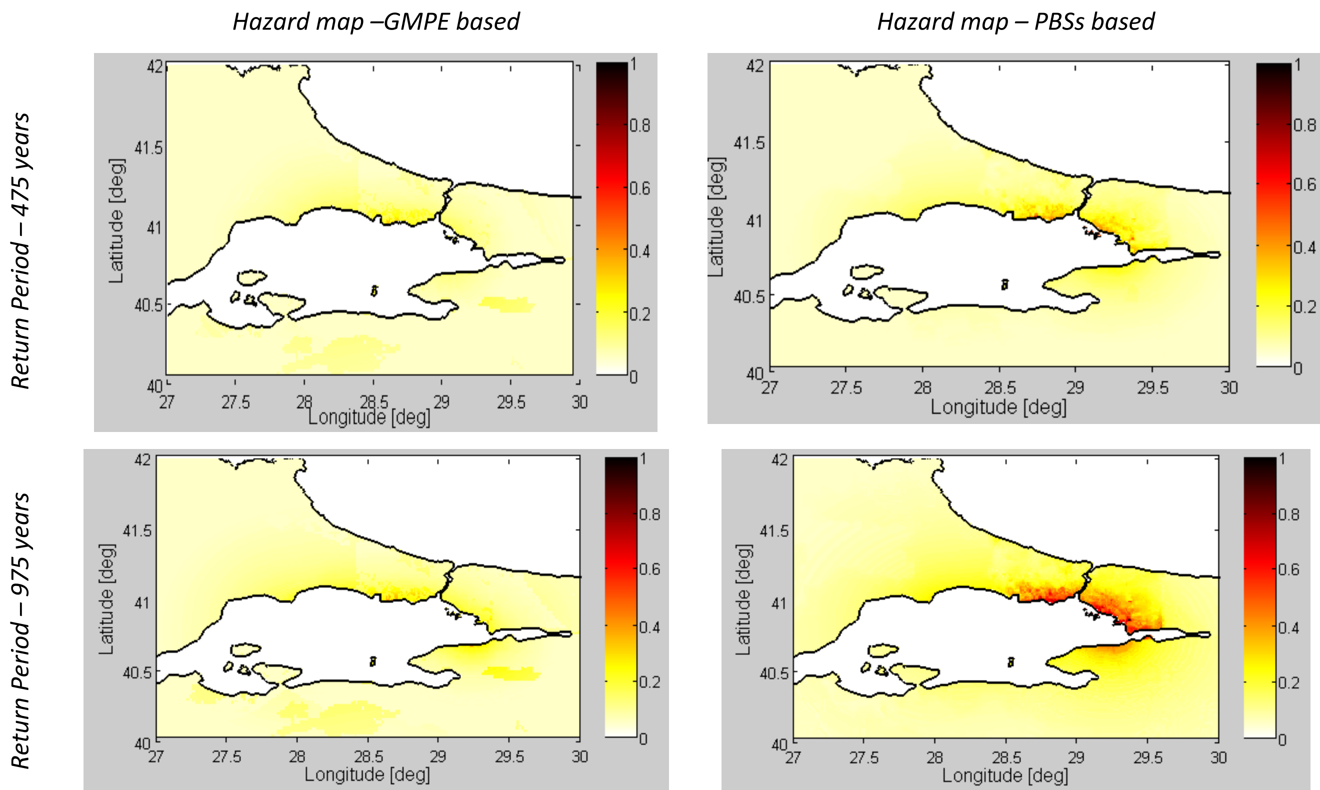

Fig. 9 – PSHA vs PSHAe: seismic hazard analyses based on classical GMPE (left hand side) or with PBSs (right-had side). The hazard maps are presented in terms of PGVgmh [m/s].

At the moment the different physics-based scenarios are equally weighted. In the future each PBS will be ranked according to the δB_{ek_TOT}, computed as previously described, in order to summarize the overall scenario effect into an easy manageable parameter. The set of PBSs will be grouped into classes and per class only one representative member will be chosen. The frequency of the class will be computed out of the proportion between the population of each class and the overall population of PBSs.

Furthermore, in order to reduce CPU time, we are planning to take advantage of the PBS but avoiding the computation of massive set of simulations each time by generalizing the previous findings in a heuristic procedure, allowing the simulation of only a limited amount of PBSs.

6. Conclusions

As presented in a companion paper submitted to the 16WCEE conference (Paolucci et al., “3D physics-based earthquake scenarios in Istanbul for seismic risk assessment”), a novel approach, largely relying on a spectral element code extensively verified ([21] and [6]) and validated ([22] and [23]), was devised in order to construct broadband seismograms.

The main methodological advancement proposed in this work aims at combining probabilistic and deterministic approaches for SHA, integrating a set of PBSs into a classical logic-tree framework, through the so-called PSHAe methodology.

In order to do that the new methodology has been shortly illustrated and a case study (Istanbul region and the nearby segment of the NAF) has been presented. A detailed analysis of the PBS generated in the area of Istanbul allowed us to draw some important conclusion on the level of ground motion expected in the region and, furthermore, the analysis of the residual provides some good hints that the reliability of the synthetic dataset produced is comparable to the one of empirical data.

The preliminary comparisons of the seismic hazard map, in terms of PGVgmh, for the Istanbul region seems to confirm the importance of taking into account PBS in the future. Further investigations are going to be performed regarding the case study of Istanbul and some additional features will be soon implemented in order to improve the proposed methodology.

Munich Re and Politecnico of Milan are jointly conducting similar studies in other areas worldwide, targeting regions characterised by high population density and exhibiting adequate geological/geothecnical/seismological information.

Finally, the present work does not represent an isolated attempt; on the contrary, it is clearly connected to an area of investigation that is of paramount importance in modern computational seismology (e.g.: [24] and [25]). Even if we realize that a more comprehensive discussion aimed at analyzing the alternative strategies/investigations would be useful, due to space constraints we refrain from addressing this topic in the present publication and instead refer the reader to future works.

7. Acknowledgements

This work has been carried out in the framework of the 2015-2017 agreement between Munich Re and Politecnico di Milano. The 3D numerical simulations were performed on FERMI cluster, at CINECA, in the framework of the ISCRA PBES4HAS project.

8. References

[1] Villani M, Faccioli E, Ordaz M, Stupazzini M (2014): High-Resolution Seismic Hazard Analysis in a Complex Geological Configuration: The Case of the Sulmona Basin in Central Italy, *Earthquake Spectra*, **30**(4), 1801-1824.

[2] Pilz M, Parolai S, Stupazzini M, Paolucci R, Zschau J (2011): Modelling basin effects on earthquake ground motion in the Santiago de Chile basin by a spectral element code, *Geophysical Journal International*, **187**(2), 929-945.

[3] Guidotti R, Stupazzini M, Smerzini C, Paolucci R, Ramieri P (2011): Numerical study on the role of basin geometry and kinematic seismic source in 3D ground motion simulation of the Mw 6.3 Lyttelton earthquake on February 21st, 2011, New Zealand, *Seismoll Res. Lett.*, **82**(6), 767-782.

[4] Smerzini C, Villani M (2012): Broadband numerical simulations in complex near field geological configurations: the case of the Mw 6.3 2009 L'Aquila earthquake, *Bulletin of Seismological Society of America*, **102**(6), 2436-2451.

[5] Bielak J, Graves R W, Olsen K B, Taborda R, Ramirez-Guzman L, Day S M, Ely G P, Roten D, Jordan T H, Maechling P J, Urbanic J, Cui Y, Juve G (2010): The ShakeOut earthquake scenario: verification of three simulation sets, *Geophysical Journal International*, **180**(1), 375-404.

[6] Mazzieri I, Stupazzini M, Guidotti R, Smerzini C (2013): SPEED: SPectral Elements in Elastodynamics with Discontinuous Galerkin: a non-conforming approach for 3D multi-scale problems, *International Journal for Numerical Methods in Engineering*, **95**(12), 991–1010.

[7] Paolucci R, Mazzieri I, Smerzini C, Stupazzini M (2014): Physics-Based Earthquake Ground Shaking Scenarios in Large Urban Areas, *Perspectives on European Earthquake Engineering and Seismology*, Geotechical, Geological and Earthquake Engineering, **34**, 331-359.

[8] Boore D M (2014): Ground-motion prediction equations: Past, present, and future, *Seismological Research Letters.* **85**

[9] Herrero A and Bernard P (1994): A kinematic self-similar rupture process for earthquakes, *Bulletin of Seismological Society of America*, **84**(4), 1216–1228.

[10] Crempien JGF, Archuleta RJ (2015): UCSB Method for Simulation of Broadband Ground Motion from Kinematic Earthquake Sources, *Seismological Research Letters*, **86** (1), 61-67.

[11] Chiou B S-J,Youngs R R (2008): An NGA model for the average horizontal component of peak ground motin and response spectra, *Earthquake Spectra*, **24**(1), 173-215.

[12] Cauzzi C, Faccioli E, Vanini M, Bianchini A (2014): Update predictive equations for broadband (0.01 to 10 s) horizontal response spectra and peak ground motions, based on a global dataset of digital acceleration records, *Bulletin of Earthquake Engineering*, **13**/6, 1578-612.

[13] Bray J D, Rodriguez-Marek A (2004): Characterization of forward-directivity ground motions in the near-fault region, *Soil Dynamics and earthquake Engineering,* **24**(2001), 815-828.

[14] Strasser FO, Abrahamson NA, Bommer JJ (2009): Sigma: issues, insights and challenges, *Seismological Research Letters* **80**(1):40–56

[15] Al Atik L, Abrahamson NA, Bommer JJ, Scherbaum F, Cotton F, Kuehn N (2010): The variability of ground motion prediction models and its components, *Seismological Research Letters*, **81**(5):794–801

[16] Gülerce Z, Kargioğlu B, Abrahamson N A (2016): Turkey-Adjusted NGA-W1 Horizontal Ground Motion Prediction Models, *Earthquake Spectra*, **32**(1), 75-100.

[17] Chen L, Faccioli E (2013): Single-standard deviation analysis of 2010-2012 strong-motion data from Canterbury region, New Zealand, *Bulletin of Earhquake Engineering*, **11**(5), 1617-1632.

[18] Faccioli E, Chen L (2012): Single-station standard deviation for probabilistic seismic hazard analyses at representative sites in the Po Plain, Northern Italy. In: *Proceedings workshop in honor and memory of Prof. Giuseppe Grandori*, November 5, 2012, Milan, Italy

[19] Cornell A C (1968): Engineering Seismic Risk Analysis, *Bulletin of the Seismological Society of America,* **58**(5), 1583-1606.

[20] Convertito V, Emolo A, Zollo A (2006): Seismic-Hazard Assessment for a Characteristic Earthquake Scenario: An Integrated Probabilistic-Deterministic Method, *Bulletin of the Seismological Society of America*, **96**(2), 377–391

[21] Chaljub E., Moczo P., Tsuno S, Bard P.Y., Kristek J., Kaser M., Stupazzini M., Kristekova M. (2010): Quantitative comparison of four numerical predictions of 3D ground motion in the Grenoble valley, France. *Bulletin of the Seismological Society of America*, **100**(4): 1427–1455.

[22] Smerzini C. and M. Villani (2012): Broadband numerical simulations in complex near field geological configurations: the case of the Mw 6.3 2009 L'Aquila earthquake, *Bulletin of Seismological Society of America*, v. 102, p. 2436–2451.

[23] Paolucci R., Mazzieri I. and Smerzini. C. (2015): Anatomy of strong ground motion: near-source records and three-dimensional physics-based numerical simulations of the Mw 6.0 2012 May 29 Po Plain earthquake, Italy, *Geophys. J. Int.* 203 (3): 2001-2020.

[24] Dreger, D. S., Beroza, G. C., Day, S. M., Goulet, C. A., Jordan, T. H., Spudich, P. A., and Stewart, J. P. (2015): Validation of the SCEC Broadband Platform V14.3 Simulation Methods Using Pseudospectral Acceleration Data, S*eismological Research Letters*, **86**(1), 39–47.

[25] Goulet, C. A., Abrahamson, N. A., Somerville, P. G., and Wooddell, K. E. (2015): The SCEC Broadband Platform Validation Exercise: Methodology for Code Validation in the Context of Seismic-Hazard Analyses, *Seismological Research Letters*, **86**(1), 17–26.